Title

Environmental pro-oxidants induce altered envelope protein profiles in human keratinocytes

Journal

Toxicological Sciences, 197(1)

ISSN

1096-6080

Authors

Lin, Lo-Wei

Durbin-Johnson, Blythe P

Rocke, David M

et al.

Publication Date

2024

DOI

10.1093/toxsci/kfad103

Peer reviewed

Environmental pro-oxidants induce altered envelope protein profiles in human keratinocytes

Lo-Wei Lin[a*], Blythe P. Durbin-Johnson[b], David M. Rocke[b], Michelle Salemi[c], Brett S. Phinney[c], Robert H. Rice[a*]

[a] Department of Environmental Toxicology, University of California, Davis, CA 95616, USA

[b] Division of Biostatistics, Department of Public Health Sciences, University of California, Davis, CA, USA

[c] Proteomics Core Facility, University of California, Davis, USA

ORCID IDs:

Lo-Wei Lin	0000-0002-0876-7826
David M. Rocke	0000-0002-3958-7318
Brett Phinney	0000-0003-3870-3302
Robert H. Rice	0000-0003-2058-4405

*Corresponding authors: Department of Environmental Toxicology, University of California, Davis, CA 95616-8588. Tel (530)752-5176; Email Lo-Wei Lin lowlin@ucdavis.edu or Robert H. Rice rhrice@ucdavis.edu

Key words: cornified envelope, covalent cross-link, oxidative stress, proteomics

Running Title: Pollutant-induced keratinocyte envelope formation

Abbreviations: CE, cornified envelope; DMNQ, 2,3-dimethoxy-1,4-naphthoquinone; MLS, mesquite liquid smoke; ROS, reactive oxygen species; TCDD, 2,3,7,8-tetrachlorodibenzo-*p*-dioxin.

Abstract

Cornified envelopes (CEs) of human epidermis ordinarily consist of transglutaminase-mediated cross-linked proteins and are essential for skin barrier function. However, in addition to enzyme-mediated isopeptide bonding, protein cross-linking could also arise from oxidative damage. Our group recently demonstrated abnormal incorporation of cellular proteins into CEs by pro-oxidants in woodsmoke. In this study, we focused on 2,3-dimethoxy-1,4-naphthoquinone (DMNQ), mesquite liquid smoke (MLS), and 2,3,7,8-tetrachlorodibenzo-*p*-dioxin (TCDD), to further understand the mechanisms through which environmental pro-oxidants induce CE formation and alter the CE proteome. CEs induced by the ionophore X537A were used for comparison. Similar to X537A, DMNQ- and MLS-induced CE formation was associated with membrane permeabilization. However, since DMNQ is non-adduct forming, its CEs were similar in protein profile to those from X537A. By contrast, MLS, rich in reactive carbonyls that can form protein adducts, caused a dramatic change in the CE proteome. TCDD-CEs were found to contain many CE precursors, such as small proline-rich proteins and late cornified envelope proteins, encoded by the epidermal differentiation complex. Since expression of these proteins is mediated by the aryl hydrocarbon receptor (AhR), and its well-known target protein, CYP1A1, was exclusively present in the TCDD group, we suggest that TCDD alters the CE proteome through persistent AhR activation. This study demonstrates the potential of environmental pro-oxidants to alter the epidermal CE proteome and indicates that the cellular redox state has an important role in CE formation.

Introduction

Skin is the first line of defense against external threats. It quenches reactive oxygen species (ROS), absorbs ultraviolet light radiation, prevents pathogen infiltration, and limits water and electrolyte loss from the body (Elias 2005; Vermeij et al. 2011). The skin barrier is established by terminally differentiated keratinocytes, also known as corneocytes. These are dead cells filled with keratins and held together by corneodesmosomes (intercellular adhesive structures). Their plasma membranes are replaced by cornified envelopes (CEs), insoluble and chemically resistant structures made from transglutaminase (TGM)-mediated cross-linked protein (Evora et al. 2021). With their attached lipids, CEs constitute a specialized hydrophobic barrier to the environment (Meyer et al. 2021).

The composition of CEs determines their biomechanical properties and influences barrier function. A large list of proteins, including filaggrin (FLG), involucrin (IVL), loricrin (LOR), and members of several protein families, such as keratin (KRT), late cornified envelope (LCE), and small proline-rich (SPRR) proteins, are known CE precursors (Karim et al. 2019b). These precursor proteins not only participate in barrier function but can also have roles in inflammatory diseases, wound healing, and mucosal defense against microbes (De Heller-Milev et al. 2000; Herman and Herman 2019; Inada et al. 2000). Disruption of these CE components can lead to the development of several skin disorders. For example, decreased expression or mutations of FLG are strong predisposing factors for atopic dermatitis (Palmer et al. 2006).A genetic basis for lamellar ichthyosis can be found in reduced TGM1 activity, which impairs the cross-linking of CE components (Huber et al. 1995; Russell et al. 1995). Moreover, the transcription of certain CE proteins changes drastically during aging, concomitant with altered skin permeability, reduced post-injury barrier recovery, and increased pathogen invasion (Rinnerthaler et al. 2013).

Environmental factors that influence barrier function and skin health include ultraviolet light radiation, air pollution, tobacco smoke, diet, and cosmetic products. Among them, air pollution is considered the world's largest environment health threat, and combustion products in polluted air can promote oxidative stress (Parrado et al. 2019). A recent study has demonstrated that abnormal CE formation occurs in cultured keratinocytes exposed to liquid smoke (LS) (Lin et al. 2021). LS is generated from smoke condensates of smoldering wood chips, a process similar to biomass burning during wildfires. Mimicking emissions from biomass burning, LS shares many chemical components with woodsmoke, including oxidative carbonyl compounds (Montazeri et al. 2013; Simon et al. 2005). These pro-oxidants and electrophiles in LS can induce oxidative stress, leading to protein damage and

protein cross-links. The LS-induced CEs were also found to have higher protein content than those induced by ionophore. Unlike TGM-catalyzed protein cross-linking, that induced by oxidative damage is less specific and can occur not only between CE precursors but also among other cellular proteins. Therefore, the previous study suggests that abnormal incorporation of cellular proteins into CEs could disrupt barrier function, revealing a mechanism through which air pollution can adversely affect the skin.

Besides air pollution, other environmental chemicals are also capable of ROS generation and can pose risks to skin health. Polycyclic aromatic hydrocarbons such as benzo(a)pyrene, found widely in the environment, are a good example (Tsuji et al. 2011). Additionally, the herbicide paraquat (1,1'-dimethyl-4,4'-bipyridinium) can cause a variety of skin diseases through redox cycling and ROS generation (Black et al. 2008). Despite the importance of CEs for skin barrier function, the impacts of environmental exposures on CE composition have hardly been studied. Here, we performed a proteomic analysis of CEs induced by exposure to three environmental pro-oxidants: (1) 2,3-dimethoxy-1,4-naphthoquinone (DMNQ), a redox cycling compound that produces ROS without adduct formation (Ross et al. 1986), (2) mesquite liquid smoke (MLS), an extract of woodsmoke condensate that is rich in reactive carbonyl compounds, and (3) 2,3,7,8-tetrachlorodibenzo-*p*-dioxin (TCDD), which causes oxidative stress through persistent activation of the aryl hydrocarbon receptor (AhR) (Reichard et al. 2006). CEs induced by these three chemicals were compared to X537A-induced CEs because calcium is a key regulator of keratinocyte differentiation (Bikle et al. 2012; Elsholz et al. 2014) and ionophore X537A (a known *in vitro* CE inducer) can permeabilize the cell membrane to extracellular calcium, activating TGMs (calcium-dependent enzymes) for protein cross-linking and CE assembly (Rice and Green 1979).

Materials and Methods

Chemicals. DMNQ (2,3-dimethoxy-1,4-naphthoquinone, purity ≥ 99%) and X537A (lasalocid, purity ≥ 98%) were purchased from Cayman Chemical, USA (items no.19571 and no. 15505). TCDD (2,3,7,8-tetrachlorodibenzo-*p*-dioxin) was purchased from the National Cancer Institute (NCI) Chemical Carcinogen Repository. MLS (Wright's Mesquite liquid smoke, USA) was purchased from local supermarkets. A recent cell-based assessment of liquid smoke has estimated that in a mouse hepatoma cell line, 24 h exposure to 0.05~0.1 µl/ml MLS is equal to exposure to 2 µM tert-butylhydroquinone (tBHQ) and could lead to 1.5-fold Nrf2 induction (compared to vehicle control). In a human breast cancer cell line, 24 h exposure to 0.05~0.1 µl/ml MLS is equal to exposure to 0.8 pM TCDD and could lead to 15% of maximal AhR activation (Selin et al. 2022).

Cell culture. Human epidermal keratinocytes (passage 5-10) were derived from a sample of ostensibly normal adult foreskin (Rice et al. 1993). These cells were grown with 3T3 feeder layer support in a 2:1 mixture of Dulbecco Vogt Eagle's and Ham's F-12 media supplemented with 5% fetal bovine serum, 0.4 µl/mg hydrocortisone, 5 µg/ml insulin, 5 µg/ml transferrin, 0.18 mM adenine, 10 ng/ml epidermal growth factor (Allen-Hoffmann and Rheinwald 1984), and 10 µM Y-27632, a Rho kinase inhibitor that increases proliferative capacity and lifespan of primary human keratinocytes while preserving their capacity to differentiate (Chapman et al. 2010).

Measurement of cornified envelopes. At confluence, keratinocytes were treated with 100 µM DMNQ, 10 µl/ml MLS, 10 nM TCDD, or 100 µM X537A in medium without epidermal growth factor or Y-27632. After desired incubation times, cells were harvested in Tris-EDTA buffer containing 2% sodium dodecyl sulfate (SDS) and 20 mM dithioerythritol, and incubated in a 70°C oven for 30 min. Once soluble proteins were dissolved, CEs (insoluble in denaturants) were collected by centrifugation for 5 min at 10,000 rpm. The CE samples were then rinsed twice with Tris-EDTA buffer containing 0.1% SDS and resuspended in this solution for quantitation. Light scattering at A^{340} was used as a measure of CE quantity as CEs are insoluble particulates that scatter light in suspension (Rice and Green 1979).

Lactate dehydrogenase (LDH) assay. LDH activity in the medium was used to monitor plasma membrane permeability following the manufacturer's protocol (Thermo Fisher Scientific). Briefly, cell culture medium was collected and incubated with LDH Substrate Mix at 37°C for 30 min. After adding the Stop Solution, the reaction product, formazan (whose level is directly proportional to the amount of LDH released into the medium), was measured at 490 nm. A^{680} value (background) was first subtracted

from the A^{490} value, and the % of LDH release was calculated using the following formula: [treatment or control value / maximum value] X 100%. The value of the maximum LDH release was obtained by treating the cells with lysis buffer.

Proteomic sample preparation. At confluence, cultured keratinocytes were treated with 100 μM DMNQ, 10 μl/ml MLS, 10 nM TCDD, or 100 μM X537A in medium without epidermal growth factor or Y-27632. TCDD requires a week to induce maximal CE formation (the others induced CE formation from nearly all the cells after one day). After 3-day (or 7-day for TCDD) incubation, cell pellets were collected, rinsed twice with phosphate-buffered saline and harvested in Tris-EDTA buffer. The samples were processed and separated into SDS-dithiothreitol soluble and insoluble (envelope) fractions as previously described (Karim et al. 2019b). Specifically, to facilitate release and removal of the solubilized proteins, pellets were extracted 4 times with 2% SDS-0.1 M sodium phosphate-50 mM dithiothreitol. Each time, the pellets were incubated in a 95 °C water bath for 5 min followed by magnetic stirring at room temperature for 30 min. After each extraction, the soluble and insoluble fractions were separated by centrifugation at 20,000 x g for 10 min. After the 4th extraction, aliquots of the first solubilized and final insoluble fractions were alkylated with 0.1 M iodoacetamide for 45 min in the dark. The solubilized proteins were recovered by ethanol precipitation. The pellets from the two fractions were then rinsed with 70% ethanol twice, resuspended in 0.05 M ammonium bicarbonate-10% acetonitrile solution, and digested with reductively methylated trypsin (~ 1% by mass). Digestion was continued for 3 days with daily additions of trypsin. Finally, the samples were clarified by centrifugation at 20,000 x g for 30 min, and the supernatants (containing the tryptic peptides) were submitted for mass spectrometric analysis.

Mass spectrometry and database searching. Peptide chromatographic separation was performed on a Dionex UltiMate 3000 RSLC system (Thermo Fisher Scientific) with a PepSep C18 column (8 cm capillary length, 150 μm inner diameter, and 1.5 μm particle size) at a flow rate of 0.5 μl/min and a multistep gradient with (A) 0.1% formic acid in water and (B) 0.1% formic acid in 80% acetonitrile. Eluted peptides were analyzed by an Orbitrap Exploris 480 mass spectrometer (Thermo Fisher Scientific). A MS scan was obtained with the following settings: scan range 350-1500 m/z, resolution 60,000, and automatic gain control target value 300%. MS/MS spectra were acquired using the top 40 method with a resolution of 15,000, automatic gain control target value of 200%, isolation width 1.5 m/z, and normalized collision energy 30%. The generated MS/MS spectra were searched against the UniProt Human Proteome (149,646 entries), appended with common laboratory contaminants and an

equal number of reverse decoy sequences, using X! Tandem Alanine (2017.2.1.4). The search was performed with settings as previously described (Karim et al. 2019a; Rice et al. 2017).

Identified peptides and proteins were validated by Scaffold (4.10.0) with <0.1% peptide decoy false discovery rate and 1.2% protein false discovery rate (two peptide minimum). Proteins with shared peptides were grouped. Spectral counts of exclusive peptides (those belonging to only one protein) were compiled and compared to weighted peptide counts (adjusted according to the number of other proteins sharing the same peptide sequence), and proteins with no or very few exclusive peptides were removed from the analysis. The Scaffold file and all raw data are available at the massive Proteomics repository (https://massive.ucsd.edu/) with MassIVE id number MSV000090901, and Proteome Exchange (http://www.proteomexchange.org/) with dataset identifier #PXD038827.

Abundance analysis. Estimates of relative protein abundance were obtained using exponentially modified protein abundance index (emPAI) calculations through the Scaffold platform. Based on empirical observations (Ishihama et al. 2005) and available as open-source software (Shinoda et al. 2010), this semi-quantitative method is commonly employed to indicate relative protein amounts and changes in their abundance. This method has previously estimated the keratin content of SDS-dithiothreitol insoluble envelope material in hair shaft (Rice et al. 2009) and nail plate (Rice et al. 2010) as ~45%.

Statistical analysis. For proteomics, proteins with less than 1 average weighted spectral count from all the samples were excluded. The weighted spectral count data were TMM (trimmed mean of M values) normalized (Robinson and Oshlack 2010) and analyzed using the limma-voom Bioconductor pipeline (limma version 3.46.0, edgeR version 3.32.1) (Ritchie et al. 2015). This pipeline log transforms and scales the count data, fits a linear model to each protein, and uses empirical Bayes smoothing (Smyth 2004) to improve estimates of standard errors of log fold changes for hypothesis testing, and adjusted the *p*-values for multiple testing using the Benjamini-Hochberg false discovery rate controlling method (Benjamini and Hochberg 1995). The model used in limma included effects for treatment, fraction, the interaction between treatment and fraction, and experiment. Log fold changes between treatments and fractions were estimated as contrasts in this model. TCDD-CEs (7 days of exposure) were compared to X537A-CEs (3 days of exposure, giving maximal envelope formation). Analyses were conducted using R (version 4.0.5). The rmd file from the limma analysis can be found in Supplementary File 1.

For cell culture experiments, comparisons between more than 2 groups were performed using one-way ANOVA with Dunnett's post hoc test to calculate individual differences. Unpaired t-testing was used to compare differences between 2 treatment groups. The analyses were performed on GraphPad Prim 9 with a significance set at $p < 0.05$.

Enrichment analysis. The official gene symbols of differentially expressed proteins were uploaded to the DAVID (**D**atabase for **A**nnotation, **V**isualization, and **I**ntegrated **D**iscovery) bioinformatics resources (https://david.ncifcrf.gov/). Enriched GO (Gene Ontology) terms associated with the protein list and the number of proteins involved in each term were generated. Modified Fisher Exact *p*-value (EASE score) was calculated to determine whether the uploaded protein list was specifically enriched in a particular GO term by more than random chance. When the entire family of tests was considered, the false discovery rate was corrected using the Benjamini-Hochberg correction.

Results

Membrane permeabilization was associated with DMNQ-, MLS-, and X537A-induced CE formation

CE formation was induced when cultured keratinocytes were exposed to DMNQ and MLS for 24 h (Figure 1A). During the exposure, cell membrane integrity was compromised, as indicated by increased LDH release (Figure 1B). However, with an exposure time of 6 h, neither CE formation nor LDH release was induced under DMNQ or MLS treatments. In contrast, exposure to positive control X537A resulted in CE formation and LDH release at both time points. Finally, it took about one week for TCDD to produce maximal CE formation but, at that time, LDH release did not increase concordantly.

Effects of calcium chelation, TGM inhibition, and antioxidant exposure on DMNQ-, MLS-, and X537A-induced CE formation

Through membrane damage and permeabilization, exposure to DMNQ could result in influx of extracellular calcium, activation of TGMs, and the subsequent enzyme-mediated protein cross-linking and CE assembly, an adverse outcome pathway similar to exposure to X537A. As shown in Figure 2A and 2B, chelating calcium with EDTA and alkylating the cysteine active site of TGMs with iodoacetamide (IA) drastically prevented both DMNQ and X537A from inducing CE formation. Despite membrane damage and permeabilization, calcium chelation and TGM inhibition did not prevent MLS from inducing CE formation. This is due to its carbonyl content capable of chemical-induced cross-linking, as previously described (Lin et al. 2021). However, once the generated ROS or reactive carbonyls were neutralized by antioxidant N-acetylcysteine (NAC), DMNQ- and MLS-induced membrane permeabilization (Figure 2C, left panel) and CE formation (Figure 2C, right panel) were decreased . In contrast, NAC did not prevent X537A from permeabilizing cell membranes or inducing CE formation because X537A does not initiate its effect through ROS generation.

The level of similarity of individual proteomic samples was visualized using multidimensional scaling (MDS)

Keratinocytes treated with DMNQ, MLS, TCDD and X537A were collected, processed, and prepared for proteomic analysis. The envelope fraction (which contains insoluble envelope proteins) and the soluble fraction (which contains solubilized cytosolic proteins) from each treatment were analyzed separately. As shown by multidimensional scaling (MDS), a two-dimensional display of sample similarity, the profiles of X537A, DMNQ, and MLS soluble fractions locate closely together, indicating

similar proteomes (Figure 3). In the envelope fractions, cells treated with X537A and DMNQ have similar protein compositions. Since MLS is capable of protein adduct formation, it produced CEs with a distinct protein profile from DMNQ-CEs, despite both acting through ROS production. Finally, the envelope and soluble protein profiles from cells treated with TCDD were isolated from those of other treatments, suggesting that TCDD altered cytosolic and envelope proteomes through a unique mechanism, potentially by long-term AhR activation.

Quantitative estimation and enrichment analysis of CE protein profiles

Protein amounts were estimated by exponentially modified protein abundance index (emPAI) calculations (Supplementary File 2), of which the top 20 are shown in Table 1. Together, these top 20 proteins account for ~80% of the total CE protein in each group. Both DMNQ- and X537A-CEs are comprised of S100 calcium-binding proteins, annexins (ANXA1 and ANXA2), small proline-rich proteins (SPRRs), and desmosomal proteins (JUP, DSP, PKP1, and PPL). In MLS-CEs, the major components are the keratins (KRTs) and glyceraldehyde 3-phosphate dehydrogenase (GAPDH), a common target of ROS due to its catalytic cysteine residue (Lazarev et al. 2016). Finally, increased levels of late cornified envelope proteins (LCEs), cornifelin (CNFN), and cysteine rich c-terminal 1 (CRCT1) were found in TCDD-CEs. Interestingly, unlike the other three groups, the top 20 proteins were more evenly distributed in amount among each constituent in TCDD-CEs.

To further characterize proteins that were differentially enriched by the environmental ROS generators, proteins in DMNQ-, MLS-, and TCDD-CEs were compared to those in X537A-CEs, and 140, 631, and 417 proteins, respectively, were found to be at least 2-fold significantly higher ($p < 0.01$). These proteins were classified by their biological process (BP) using gene ontology (GO) enrichment analysis. Sorting by adjusted *p*-values, the top five GO-BP terms from each treatment are shown in Figure 4. In DMNQ-CEs, only three GO-BP terms were statistically significant. The proteins enriched by MLS are involved in various biological processes, including tRNA aminoacylation, tricarboxylic acid cycle, protein folding, intermediate filament organization, and fatty acid beta-oxidation. In TCDD-CEs, the enriched proteins mainly function in keratinization, protein folding, proteasome-mediated ubiquitin-dependent protein catabolic processes, intermediate filament organization, and glycolysis. Statistical comparisons of all 2727 proteins between the ROS generators and X537A are found in Supplementary File 3.

Profiles of CE precursors

A list of 166 previously identified CE precursors was compiled from GO Annotations: cornified envelope (GO:0001533, cellular component), keratinization (GO:0031424, biological process), and keratinocyte differentiation (GO:0030216, biological process). In addition, KPRP, KRT13, and KRT14 were recently discovered in human stratum corneum by proteomics and were thus added to the list (Karim et al. 2019b). When searched against this list, 92 precursors were found in our datasets, and together comprised 50%, 45%, 64%, and 69% of the X537A-, DMNQ-, MLS-, and TCDD-CEs, respectively. Table 2 lists CE precursors that comprised ≥ 0.5% of the total CE proteins. Precursors in DMNQ-CEs differed little from X537A-CEs. MLS-CEs contained substantial amounts of keratin and very few SPRRs and desmosomal proteins. Finally, TCDD-CEs had more diversified precursors, and many of them (e.g., SPRRs and LCEs) are encoded in the epidermal differentiation complex (EDC) (Kypriotou et al. 2012). The list of 166 CE precursors and details of the search results are found in Supplementary File 4.

While ionophore-induced CE formation is a valuable model for examining envelope formation in keratinocytes, present results reflect the incomplete degree of cell maturation in culture. As shown in Figure 5, keratins comprised nearly 40% of the total soluble cytosolic protein in treated cultures. This is similar to previous measurements when the culture system was first established and much lower than the 85% of total protein extractable from in human callus (Sun and Green 1978). By contrast, the keratin content in CEs induced by X537A and DMNQ was ~2% compared to ~70% observed in CEs from callus (Karim et al. 2019b). The cultured cells express only a low level of certain differentiation features, such as the non-membrane-bound TGM3 (0.1% the level of TGM1 compared to 25% in epidermis) (Supplementary Table S4C), which we speculate augments TGM1-cross-linked structures with keratins. Remarkably, CEs induced by MLS and TCDD were nearly 50% and 15% keratin, respectively, although neither treatment induces keratin expression (Hu et al. 2013; Lin et al. 2021). These findings indicate the considerable vulnerability of CE to modification of their protein profiles by such treatment.

Mitochondrial proteins were cross-linked by MLS into CEs

Mitochondrial (Mt) proteins are sensitive to oxidative damage. To further assess the impact of ROS generators on Mt proteins, we searched our datasets against GO annotation mitochondrion (GO: 0005739 cellular component) and identified 67 Mt proteins. Quantitatively, these Mt proteins account for about 1% of the total solubilized cytosolic protein among all four treatments. In the envelope fraction, these Mt proteins account for 0.14%, 0.14%, 0.67%, and 0.09% of the total protein in X537A,

DMNQ, MLS, and TCDD group, respectively. When compared to X537A-CEs, 2, 40, and 19 of these 67 Mt proteins were increased at least 2-fold ($p < 0.01$) by DMNQ, MLS, and TCDD (Figure 6). These findings indicate that, compared to CEs induced by non-ROS generator X537A, DMNQ incorporated very few Mt proteins into the envelopes. In MLS-CEs, however, a considerable number of Mt proteins were targeted for incorporation, resulting in a significant increase of Mt protein level in the CEs ($p < 0.0001$). Finally, although the level of Mt proteins did not increase in the TCDD group ($p = 0.33$), 19 out of 67 Mt proteins were differentially enriched, suggesting that TCDD was incorporating a different profile of Mt proteins into the CEs. Nevertheless, this result demonstrates that Mt proteins are targets of MLS-mediated protein cross-linking, which is consistent with GO-BP analysis (Figure 4) since biological processes such as tRNA aminoacylation, protein folding, tricarboxylic acid cycle, and beta-oxidation occur in mitochondria. The list of Mt proteins and details of the search results can be found in Supplementary File 5.

Presence of CYP1A1 protein in TCDD-CEs

Since cellular proteins can be targeted by pro-oxidative chemicals and be abnormally incorporated into CEs, we next examined whether proteins of AhR target genes could alter CE proteome. A list of AhR downstream genes was compiled from previous studies using cDNA microarray, RNA-sequencing, and meta-analysis on human cell cultures exposed to TCDD (Kim et al. 2009; Oshchepkova et al. 2020; Teino et al. 2020) (Supplementary File 6). As shown in Figure 7, proteins of well-known AhR target genes CYP1A1 and ALDH1A3 were enriched significantly in both TCDD envelope and soluble fractions. The lack of proteins of other AhR target genes, such as CYP1B1 or AHRR, can be attributed at least partly to the relatively small dynamic range of untargeted proteomics, where many proteins are too low in amount to be detected, compared to next generation sequencing. Nevertheless, despite small relative quantities (0.03% and 0.01% of the total soluble and envelope protein in the TCDD group), the presence of CYP1A1 protein still demonstrates the abnormal incorporation of non-CE precursors into the CEs by environmental chemicals.

Discussion

The formation of covalent cross-links within or between proteins can profoundly impact their conformation and biological properties, such as turnover or activity. While some of these cross-links are formed enzymatically and are essential in stabilizing or maintaining protein structure and function (e.g., TGM-mediated cross-links), others that are generated as a consequence of oxidant exposure are potentially harmful to the cell (Fuentes-Lemus et al. 2021). These undesired protein cross-links could end up as targets of proteasomal degradation. However, if the proteasomal system is overwhelmed and deactivated by oxidative stress, the unwanted cross-links could accumulate, altering the cellular proteome (Jung et al. 2014). Moreover, protein adducts of exogenous chemicals can stimulate the immune system, leading to inflammation and allergic sensitization (Natsch et al. 2012).

The actions through which chemicals induce CE formation could have great impact on the CE protein profiles. It is likely that DMNQ induces CE formation through ROS-mediated membrane permeabilization, allowing calcium influx to activate TGMs for protein cross-linking. Since DMNQ is non-alkylating and non-adduct forming, it produced CEs with profile similar to that induced by X537A. Although MLS-induced CE formation was also associated with membrane permeabilization, MLS does not rely solely on TGMs for protein cross-linking. A carbonyl can form an adduct with a protein side chain and further reaction with another protein side chain can produce a cross-linked species (Hagglund et al. 2018). Therefore, MLS-CEs appear to result from both TGM- and chemical-induced protein cross-linking through cell membrane permeabilization and oxidative damage to cellular proteins (Lin et al. 2021).

Unlike TGM-mediated cross-linking, oxidative cross-linking is less specific and can incorporate various proteins that are vulnerable to oxidative damage. Among them, Mt proteins were found to be one of the main targets. Because Mt proteins are rich in cysteine residues, the concentration of exposed protein thiols within the mitochondrial matrix is estimated to be 20 to 25- fold higher than that of glutathione in the same compartment (Requejo et al. 2010). These exposed protein thiols, comprising an antioxidant defense against ROS generated from the respiratory chain, could also turn the mitochondria into targets of environmental oxidant pollutants due to the rapid reaction of thiols with ROS and electrophiles.

AhR is a ligand-dependent transcription factor that responds to exogenous and endogenous stimulants by inducing expression of a variety of target genes (Denison et al. 2011). Beyond its role in xenobiotic metabolism, AhR is also an important regulator of skin barrier formation (Fernandez-Gallego et al.

2021; Furue et al. 2014), and triggers the expression of genes in the epidermal differentiation complex (Sutter et al. 2011). Consistent with our proteomic profiling, many CE precursors from the complex were substantially enriched in the TCDD group. However, prolonged AhR activation can cause exaggerated acceleration of keratinocyte terminal differentiation, leading to exacerbated keratinization (Furue and Tsuji 2019). As demonstrated by our GO-BP analysis, the most significant enriched protein category in the TCDD group is keratinization.

The detailed mechanism through which TCDD activates TGM for CE assembly remains unclear, and it is unlikely through plasma membrane permeabilization. A possible mechanism could be disruption of the intracellular calcium homeostasis as reported by previous studies in other cell types (Morales-Hernandez et al. 2012; Rainey et al. 2017). ROS production can also be a contributor as antioxidants, such as quercetin and NAC, were shown to abrogate the effect of TCDD to promote CE formation (Kennedy et al. 2013). Overexpression of CYP1A1 is considered to an important source of intracellular ROS, and siRNA knockdown of CYP1A1 was shown to reduce ROS production in human endothelial cells treated with TCDD (Kopf and Walker 2010). In our study, TCDD stimulated CE formation slowly, suggesting long-term alterations are required for TCDD to elicit toxicity and disrupt important cell functions, such as calcium or redox homeostasis.

Cross-linking is often seen in oxidatively damaged proteins and aggregates (Levy et al. 2019). Targets of such cross-linking are proteins that are available or vulnerable to oxidative attack or modification. Decades ago, the precursor availability model (also known as the dustbin hypothesis) explained molecular details regarding CE formation (Michel et al. 1987; Robinson et al. 1997). In this model, the authors speculated that proteins, regardless of their roles in other cellular processes, can potentially function as CE components depending on (a) the precursors that are available at the time of cross-linking and (b) the types of TGMs present and their interactions with the specific cross-linking sites on the target proteins. The present study indicates the importance of a cellular redox environment that supplies oxidatively damaged proteins. For example, despite DMNQ-CEs sharing similar protein profiles with X537A-CEs, one of the top 20 abundant proteins, beta-actin (ACTB), was increased to 9% by DMNQ (vs. 2.3% in X537A-CEs) (Table 1). This can be attributed to different levels of oxidative status as beta-actin can be oxidized by ROS (normally, this modification is essential for cytoskeleton organization) (Fiaschi et al. 2006). In MLS-CEs, the most enriched proteins are the keratins. This could be due to their abundance in the cells and thereby, a high chance of interaction with the reactive carbonyls and being oxidatively modified. Finally, CYP1A1 is unlikely a substrate of TGMs because it is not as abundant as SPRRs or LCEs (other proteins induced after AhR activation) in TCDD-CEs. Yet,

the presence of CYP1A1 protein in the envelope fraction suggests other mechanisms, such as oxidative cross-linking, could play a role.

Studies in neurodegenerative diseases and premature senescence have revealed that certain proteins are more prone to oxidative damage and subsequent intracellular accumulation (Le Boulch et al. 2018; Martinez et al. 2010). These proteins are classified into several functional groups, including (1) glycolysis and energy metabolism, (2) cytoskeleton, (3) chaperones, and (4) members of the ubiquitin-proteasome system, in line with our findings (Figure 4). The accumulation of unwanted protein cross-links has been associated with aging and the progression of many human diseases (Levy et al. 2019; Reeg and Grune 2015). In the case of skin, as demonstrated by the current study, oxidative cross-linking can alter the CE proteome, a mechanism by which pro-oxidative environmental pollutants could exacerbate development of adverse cutaneous conditions.

Acknowledgements

We thank Dr. Noreen Karim for her generous advice on sample and data processing, and Dr. Allison Ehrlich for her invaluable feedback on this manuscript. We are also grateful for Shing-Jiuan Liu (Department of Electrical and Computer Engineering, University of California Davis) for her kind help with data cleaning. This research was supported by grants T32 ES07059 and UL1 TR001860 from the NIH and CA-D-ETX-2152-H from the USDA. Mass spectrometry was supported by NIH S10OD026918-01A1.

References

Allen-Hoffmann BL, Rheinwald JG. 1984. Polycyclic aromatic hydrocarbon mutagenesis of human epidermal keratinocytes in culture. Proc Natl Acad Sci U S A. 81(24):7802-7806.

Benjamini Y, Hochberg Y. 1995. Controlling the false discovery rate: A practical and powerful approach to multiple testing. Journal of the Royal Statistical Society: Series B (Methodological). 57(1):289-300.

Bikle DD, Xie Z, Tu CL. 2012. Calcium regulation of keratinocyte differentiation. Expert Rev Endocrinol Metab. 7(4):461-472.

Black AT, Gray JP, Shakarjian MP, Laskin DL, Heck DE, Laskin JD. 2008. Increased oxidative stress and antioxidant expression in mouse keratinocytes following exposure to paraquat. Toxicol Appl Pharmacol. 231(3):384-392.

Chapman S, Liu X, Meyers C, Schlegel R, McBride AA. 2010. Human keratinocytes are efficiently immortalized by a rho kinase inhibitor. J Clin Invest. 120(7):2619-2626.

De Heller-Milev M, Huber M, Panizzon R, Hohl D. 2000. Expression of small proline rich proteins in neoplastic and inflammatory skin diseases. Br J Dermatol. 143(4):733-740.

Denison MS, Soshilov AA, He G, DeGroot DE, Zhao B. 2011. Exactly the same but different: Promiscuity and diversity in the molecular mechanisms of action of the aryl hydrocarbon (dioxin) receptor. Toxicol Sci. 124(1):1-22.

Elias PM. 2005. Stratum corneum defensive functions: An integrated view. J Invest Dermatol. 125(2):183-200.

Elsholz F, Harteneck C, Muller W, Friedland K. 2014. Calcium--a central regulator of keratinocyte differentiation in health and disease. Eur J Dermatol. 24(6):650-661.

Evora AS, Adams MJ, Johnson SA, Zhang Z. 2021. Corneocytes: Relationship between structural and biomechanical properties. Skin Pharmacol Physiol. 34(3):146-161.

Fernandez-Gallego N, Sanchez-Madrid F, Cibrian D. 2021. Role of ahr ligands in skin homeostasis and cutaneous inflammation. Cells. 10(11).

Fiaschi T, Cozzi G, Raugei G, Formigli L, Ramponi G, Chiarugi P. 2006. Redox regulation of beta-actin during integrin-mediated cell adhesion. J Biol Chem. 281(32):22983-22991.

Fuentes-Lemus E, Hagglund P, Lopez-Alarcon C, Davies MJ. 2021. Oxidative crosslinking of peptides and proteins: Mechanisms of formation, detection, characterization and quantification. Molecules. 27(1).

Furue M, Takahara M, Nakahara T, Uchi H. 2014. Role of ahr/arnt system in skin homeostasis. Arch Dermatol Res. 306(9):769-779.

Furue M, Tsuji G. 2019. Chloracne and hyperpigmentation caused by exposure to hazardous aryl hydrocarbon receptor ligands. Int J Environ Res Public Health. 16(23).

Hagglund P, Mariotti M, Davies MJ. 2018. Identification and characterization of protein cross-links induced by oxidative reactions. Expert Rev Proteomics. 15(8):665-681.

Herman A, Herman AP. 2019. Antimicrobial peptides activity in the skin. Skin Res Technol. 25(2):111-117.

Hu Q, Rice RH, Qin Q, Phinney BS, Eigenheer RA, Bao W, Zhao B. 2013. Proteomic analysis of human keratinocyte response to 2,3,7,8-tetrachlorodibenzo-p-dioxin (tcdd) exposure. J Proteome Res. 12(11):5340-5347.

Huber M, Rettler I, Bernasconi K, Frenk E, Lavrijsen SP, Ponec M, Bon A, Lautenschlager S, Schorderet DF, Hohl D. 1995. Mutations of keratinocyte transglutaminase in lamellar ichthyosis. Science. 267(5197):525-528.

Inada R, Matsuki M, Yamada K, Morishima Y, Shen SC, Kuramoto N, Yasuno H, Takahashi K, Miyachi Y, Yamanishi K. 2000. Facilitated wound healing by activation of the transglutaminase 1 gene. Am J Pathol. 157(6):1875-1882.

Ishihama Y, Oda Y, Tabata T, Sato T, Nagasu T, Rappsilber J, Mann M. 2005. Exponentially modified protein abundance index (empai) for estimation of absolute protein amount in proteomics by the number of sequenced peptides per protein. Mol Cell Proteomics. 4(9):1265-1272.

Jung T, Hohn A, Grune T. 2014. The proteasome and the degradation of oxidized proteins: Part ii - protein oxidation and proteasomal degradation. Redox Biol. 2:99-104.

Karim N, Durbin-Johnson B, Rocke DM, Salemi M, Phinney BS, Naeem M, Rice RH. 2019a. Proteomic manifestations of genetic defects in autosomal recessive congenital ichthyosis. J Proteomics. 201:104-109.

Karim N, Phinney BS, Salemi M, Wu PW, Naeem M, Rice RH. 2019b. Human stratum corneum proteomics reveals cross-linking of a broad spectrum of proteins in cornified envelopes. Exp Dermatol. 28(5):618-622.

Kennedy LH, Sutter CH, Leon Carrion S, Tran QT, Bodreddigari S, Kensicki E, Mohney RP, Sutter TR. 2013. 2,3,7,8-tetrachlorodibenzo-p-dioxin-mediated production of reactive oxygen species is an essential step in the mechanism of action to accelerate human keratinocyte differentiation. Toxicol Sci. 132(1):235-249.

Kim S, Dere E, Burgoon LD, Chang CC, Zacharewski TR. 2009. Comparative analysis of ahr-mediated tcdd-elicited gene expression in human liver adult stem cells. Toxicol Sci. 112(1):229-244.

Kopf PG, Walker MK. 2010. 2,3,7,8-tetrachlorodibenzo-p-dioxin increases reactive oxygen species production in human endothelial cells via induction of cytochrome p4501a1. Toxicol Appl Pharmacol. 245(1):91-99.

Kypriotou M, Huber M, Hohl D. 2012. The human epidermal differentiation complex: Cornified envelope precursors, s100 proteins and the 'fused genes' family. Exp Dermatol. 21(9):643-649.

Lazarev VF, Nikotina AD, Semenyuk PI, Evstafyeva DB, Mikhaylova ER, Muronetz VI, Shevtsov MA, Tolkacheva AV, Dobrodumov AV, Shavarda AL et al. 2016. Small molecules preventing gapdh aggregation are therapeutically applicable in cell and rat models of oxidative stress. Free Radic Biol Med. 92:29-38.

Le Boulch M, Ahmed EK, Rogowska-Wrzesinska A, Baraibar MA, Friguet B. 2018. Proteome oxidative carbonylation during oxidative stress-induced premature senescence of wi-38 human fibroblasts. Mech Ageing Dev. 170:59-71.

Levy E, El Banna N, Baille D, Heneman-Masurel A, Truchet S, Rezaei H, Huang ME, Beringue V, Martin D, Vernis L. 2019. Causative links between protein aggregation and oxidative stress: A review. Int J Mol Sci. 20(16).

Lin L-W, Denison MS, Rice RH. 2021. Woodsmoke extracts cross-link proteins and induce cornified envelope formation without stimulating keratinocyte terminal differentiation. Toxicological Sciences. 183(1):128-138.

Martinez A, Portero-Otin M, Pamplona R, Ferrer I. 2010. Protein targets of oxidative damage in human neurodegenerative diseases with abnormal protein aggregates. Brain Pathol. 20(2):281-297.

Meyer JM, Crumrine D, Schneider H, Dick A, Schmuth M, Gruber R, Radner FPW, Grond S, Wakefield JS, Mauro TM et al. 2021. Unbound corneocyte lipid envelopes in 12r-lipoxygenase deficiency support a specific role in lipid-protein cross-linking. Am J Pathol.

Michel S, Schmidt R, Robinson SM, Shroot B, Reichert U. 1987. Identification and subcellular distribution of cornified envelope precursor proteins in the transformed human keratinocyte line sv-k14. J Invest Dermatol. 88(3):301-305.

Montazeri N, Oliveira AC, Himelbloom BH, Leigh MB, Crapo CA. 2013. Chemical characterization of commercial liquid smoke products. Food Sci Nutr. 1(1):102-115.

Morales-Hernandez A, Sanchez-Martin FJ, Hortigon-Vinagre MP, Henao F, Merino JM. 2012. 2,3,7,8-tetrachlorodibenzo-p-dioxin induces apoptosis by disruption of intracellular calcium homeostasis in human neuronal cell line shsy5y. Apoptosis. 17(11):1170-1181.

Natsch A, Gfeller H, Haupt T, Brunner G. 2012. Chemical reactivity and skin sensitization potential for benzaldehydes: Can schiff base formation explain everything? Chem Res Toxicol. 25(10):2203-2215.

Oshchepkova E, Sizentsova Y, Wiebe D, Mironova V, Kolchanov N. 2020. Meta-analysis of transcriptome data detected new potential players in response to dioxin exposure in humans. Int J Mol Sci. 21(21).

Palmer CN, Irvine AD, Terron-Kwiatkowski A, Zhao Y, Liao H, Lee SP, Goudie DR, Sandilands A, Campbell LE, Smith FJ et al. 2006. Common loss-of-function variants of the epidermal barrier protein filaggrin are a major predisposing factor for atopic dermatitis. Nat Genet. 38(4):441-446.

Parrado C, Mercado-Saenz S, Perez-Davo A, Gilaberte Y, Gonzalez S, Juarranz A. 2019. Environmental stressors on skin aging. Mechanistic insights. Frontiers in pharmacology. 10:759.

Rainey NE, Saric A, Leberre A, Dewailly E, Slomianny C, Vial G, Zeliger HI, Petit PX. 2017. Synergistic cellular effects including mitochondrial destabilization, autophagy and apoptosis following low-level exposure to a mixture of lipophilic persistent organic pollutants. Sci Rep. 7(1):4728.

Reeg S, Grune T. 2015. Protein oxidation in aging: Does it play a role in aging progression? Antioxid Redox Signal. 23(3):239-255.

Reichard JF, Dalton TP, Shertzer HG, Puga A. 2006. Induction of oxidative stress responses by dioxin and other ligands of the aryl hydrocarbon receptor. Dose Response. 3(3):306-331.

Requejo R, Hurd TR, Costa NJ, Murphy MP. 2010. Cysteine residues exposed on protein surfaces are the dominant intramitochondrial thiol and may protect against oxidative damage. FEBS J. 277(6):1465-1480.

Rice RH, Durbin-Johnson BP, Salemi M, Schwartz ME, Rocke DM, Phinney BS. 2017. Proteomic profiling of pachyonychia congenita plantar callus. J Proteomics. 165:132-137.

Rice RH, Green H. 1979. Presence in human epidermal cells of a soluble protein precursor of the cross-linked envelope: Activation of the cross-linking by calcium ions. Cell. 18(3):681-694.

Rice RH, Rocke DM, Tsai HS, Silva KA, Lee YJ, Sundberg JP. 2009. Distinguishing mouse strains by proteomic analysis of pelage hair. J Invest Dermatol. 129(9):2120-2125.

Rice RH, Steinmann KE, deGraffenried LA, Qin Q, Taylor N, Schlegel R. 1993. Elevation of cell cycle control proteins during spontaneous immortalization of human keratinocytes. Mol Biol Cell. 4(2):185-194.

Rice RH, Xia Y, Alvarado RJ, Phinney BS. 2010. Proteomic analysis of human nail plate. J Proteome Res. 9(12):6752-6758.

Rinnerthaler M, Duschl J, Steinbacher P, Salzmann M, Bischof J, Schuller M, Wimmer H, Peer T, Bauer JW, Richter K. 2013. Age-related changes in the composition of the cornified envelope in human skin. Exp Dermatol. 22(5):329-335.

Ritchie ME, Phipson B, Wu D, Hu Y, Law CW, Shi W, Smyth GK. 2015. Limma powers differential expression analyses for rna-sequencing and microarray studies. Nucleic Acids Res. 43(7):e47.

Robinson MD, Oshlack A. 2010. A scaling normalization method for differential expression analysis of rna-seq data. Genome Biol. 11(3):R25.

Robinson NA, Lapic S, Welter JF, Eckert RL. 1997. S100a11, s100a10, annexin i, desmosomal proteins, small proline-rich proteins, plasminogen activator inhibitor-2, and involucrin are components of the cornified envelope of cultured human epidermal keratinocytes. J Biol Chem. 272(18):12035-12046.

Ross D, Thor H, Threadgill MD, Sandy MS, Smith MT, Moldeus P, Orrenius S. 1986. The role of oxidative processes in the cytotoxicity of substituted 1,4-naphthoquinones in isolated hepatocytes. Arch Biochem Biophys. 248(2):460-466.

Russell LJ, DiGiovanna JJ, Rogers GR, Steinert PM, Hashem N, Compton JG, Bale SJ. 1995. Mutations in the gene for transglutaminase 1 in autosomal recessive lamellar ichthyosis. Nat Genet. 9(3):279-283.

Selin E, Mandava G, Vilcu AL, Oskarsson A, Lundqvist J. 2022. An in vitro-based hazard assessment of liquid smoke food flavourings. Arch Toxicol. 96(2):601-611.

Shinoda K, Tomita M, Ishihama Y. 2010. Empai calc--for the estimation of protein abundance from large-scale identification data by liquid chromatography-tandem mass spectrometry. Bioinformatics. 26(4):576-577.

Simon R, de la Calle B, Palme S, Meier D, Anklam E. 2005. Composition and analysis of liquid smoke flavouring primary products. J Sep Sci. 28(9-10):871-882.

Smyth GK. 2004. Linear models and empirical bayes methods for assessing differential expression in microarray experiments. Stat Appl Genet Mol Biol. 3:Article3.

Sun TT, Green H. 1978. Keratin filaments of cultured human epidermal cells. Formation of intermolecular disulfide bonds during terminal differentiation. J Biol Chem. 253(6):2053-2060.

Sutter CH, Bodreddigari S, Campion C, Wible RS, Sutter TR. 2011. 2,3,7,8-tetrachlorodibenzo-p-dioxin increases the expression of genes in the human epidermal differentiation complex and accelerates epidermal barrier formation. Toxicol Sci. 124(1):128-137.

Teino I, Matvere A, Pook M, Varik I, Pajusaar L, Uudekull K, Vaher H, Trei A, Kristjuhan A, Org T et al. 2020. Impact of ahr ligand tcdd on human embryonic stem cells and early differentiation. Int J Mol Sci. 21(23).

Tsuji G, Takahara M, Uchi H, Takeuchi S, Mitoma C, Moroi Y, Furue M. 2011. An environmental contaminant, benzo(a)pyrene, induces oxidative stress-mediated interleukin-8 production in human keratinocytes via the aryl hydrocarbon receptor signaling pathway. J Dermatol Sci. 62(1):42-49.

Vermeij WP, Alia A, Backendorf C. 2011. Ros quenching potential of the epidermal cornified cell envelope. J Invest Dermatol. 131(7):1435-1441.

Table 1. Top 20 CE proteins estimated by exponentially modified protein abundance index (emPAI).

X537A		DMNQ		MLS		TCDD	
Gene Name	% of Total	Gene Name	% of Total	Gene Name	% of Total	Gene Name	% of Total
S100A11	10.4	S100A11	9.0	KRT5	9.4	LCE3D	5.5
ANXA1	10.4	ANXA1	9.0	KRT6A	9.4	S100A11	5.5
S100A10	10.4	S100A10	9.0	KRT16	9.4	SPRR1A	5.5
S100A16	10.4	S100A16	9.0	KRT13	9.4	ANXA1	5.5
SPRR1B	10.4	ACTB	9.0	ACTB	9.4	SPRR1B	5.5
SPRR1A	7.3	SERPINB2	7.8	KRT4	8.7	S100A10	5.5
SERPINB2	5.7	SPRR1B	7.0	GAPDH	6.7	S100A16	5.5
JUP	3.8	SPRR1A	6.1	KRT14	6.5	LCE3E	5.5
DSP	2.6	DSP	3.1	KRT10	4.5	ACTB	5.5
ACTB	2.3	JUP	2.8	ANXA1	1.7	KRT6A	5.4
PKP1	2.1	HSPB1	2.5	HSPB1	1.6	SPRR2D	4.7
HSPB1	1.1	PKP1	1.8	ANXA2	1.2	SERPINB2	4.6
IVL	1.0	IVL	0.9	PPIA	1.1	KRT5	3.8
HNRNPA2B1	0.7	HNRNPA2B1	0.8	LGALS7	0.9	KRT16	3.1
ANXA2	0.7	ANXA2	0.7	PKM	0.8	KRT14	2.5
PPL	0.6	GAPDH	0.6	S100A10	0.7	JUP	2.4
SPRR2D	0.6	PPL	0.6	S100A11	0.7	IVL	2.2
KRT5	0.5	SPRR2D	0.4	KRT19	0.6	CNFN	2.0
KRT6A	0.5	KRT6A	0.4	TUBB4B	0.5	CRCT1	1.7
HNRNPA1	0.4	EEF1A1P5	0.4	KRT1	0.5	LCE1A	1.6

Table 2. CE precursors comprised more than 0.5% of the total envelope proteins.

X537A		DMNQ		MLS		TCDD	
Gene Name	% of Total	Gene Name	% of Total	Gene Name	% of Total	Gene Name	% of Total
Annexin							
ANXA1	10.4	ANXA1	9.0	ANXA1	1.7	ANXA1	5.5
ANXA2	0.7	ANXA2	0.7	ANXA2	1.2		
Small Proline-Rich Protein							
SPRR1A	7.3	SPRR1A	6.1			SPRR1A	5.5
SPRR1B	10.4	SPRR1B	7.0			SPRR1B	5.5
SPRR2D	0.6					SPRR2A	0.9
						SPRR2D	4.7
						SPRR2G	0.8
Serpin							
SERPINB2	5.7	SERPINB2	7.8			SERPINB2	4.6
Desmosomal Protein							
DSP	2.6	DSP	3.1			DSP	1.0
JUP	3.8	JUP	2.8			JUP	2.4
PKP1	2.1	PKP1	1.8			PKP1	0.8
PPL	0.6	PPL	0.6				
Keratin							
				KRT4	8.7	KRT5	3.8
				KRT5	9.4	KRT6A	5.4
				KRT6A	9.4	KRT10	0.6
				KRT10	4.5	KRT14	2.5
				KRT13	9.4	KRT16	3.1
				KRT14	6.5		
				KRT16	9.4		
Late Cornified Envelope Protein							
						LCE1A	1.6
						LCE3D	5.5
						LCE3E	5.5
						LCE1F	0.8
Others							
HSPB1	1.1	HSPB1	2.5	HSPB1	1.6	CNFN	2.0
IVL	1.0	IVL	0.9			CRCT1	1.7
						IVL	2.2

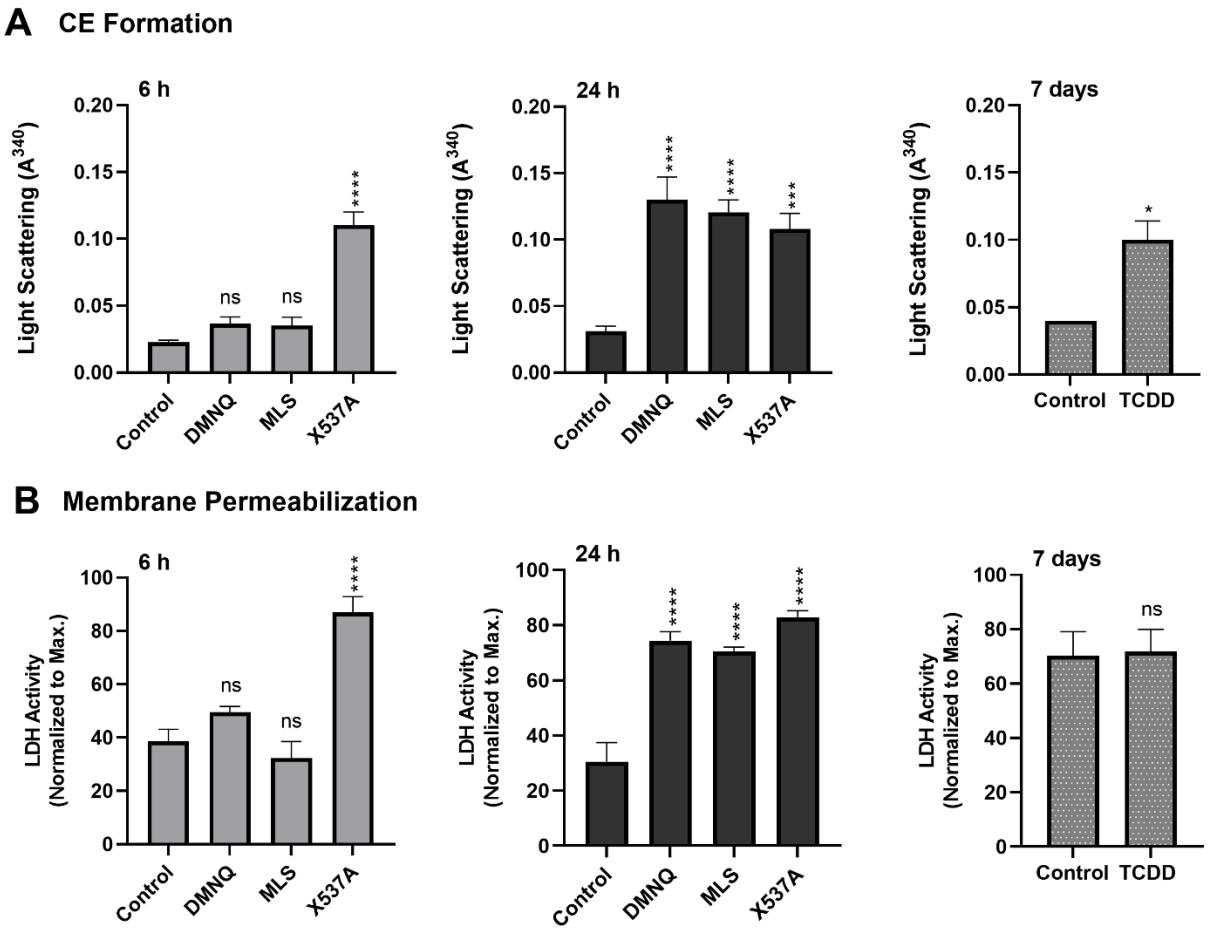

Figure 1. Measure of cell membrane integrity at the time of CE formation. Keratinocytes were treated with 100 µM DMNQ, 10 µl/ml MLS, or 100 µM X537A for indicated time. After exposures, (A) CEs were harvested for quantitation and (B) culture media were collected for LDH assay. In the TCDD group, media were changed once on Day 4, and the high LDH activity in its control could be due to the accumulation of spontaneous LDH release from Day 4 to Day 7. Each figure shows results from three independent experiments. Significances are indicated (ns, not significantly different; *, $p < 0.05$; **, $p < 0.01$; ***, $p < 0.001$; ****, $p < 0.0001$).

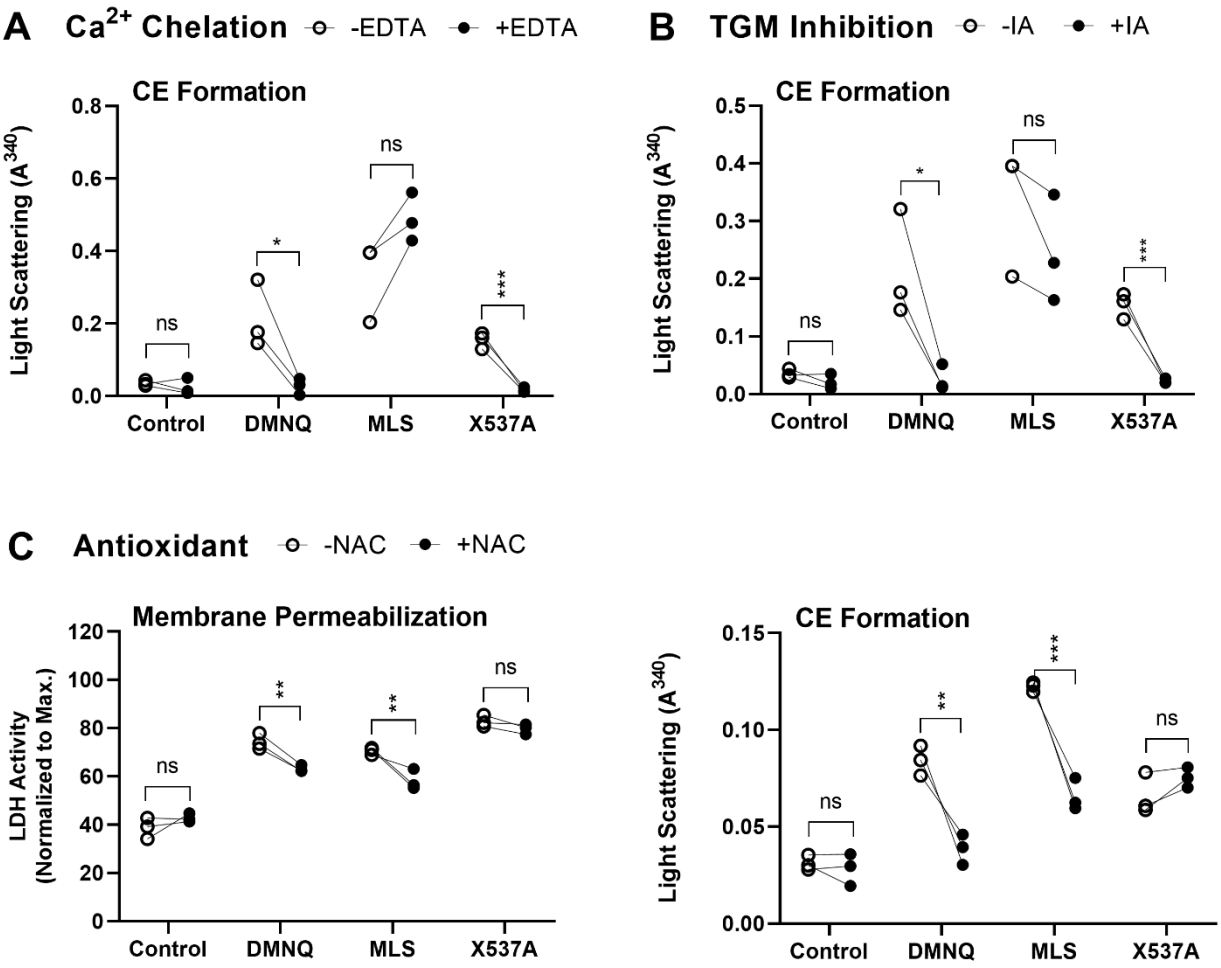

Figure 2. Effects of calcium chelation, TGM inhibition, and antioxidant on CE formation and membrane permeabilization. (A) Cells were treated as indicated ± 1 mM EDTA. The calcium concentration was estimated to be ~1 mM in DMEM/F-12 medium and 1 mM EDTA chelated most of the calcium in the medium. (B) Cells were pretreated ± 20 mM IA. After 1 h, they were switched to fresh medium containing the indicated chemicals. (C) Cells were preloaded ± 10 mM N-acetylcysteine (NAC) for 1 h before chemical exposures. The incubation time of all the experiment was 24 h before CE quantitation or LDH measurement. Each figure shows results from three independent experiments. Significances are indicated (ns, not significantly different; *, $p < 0.05$; **, $p < 0.01$; ***, $p < 0.001$).

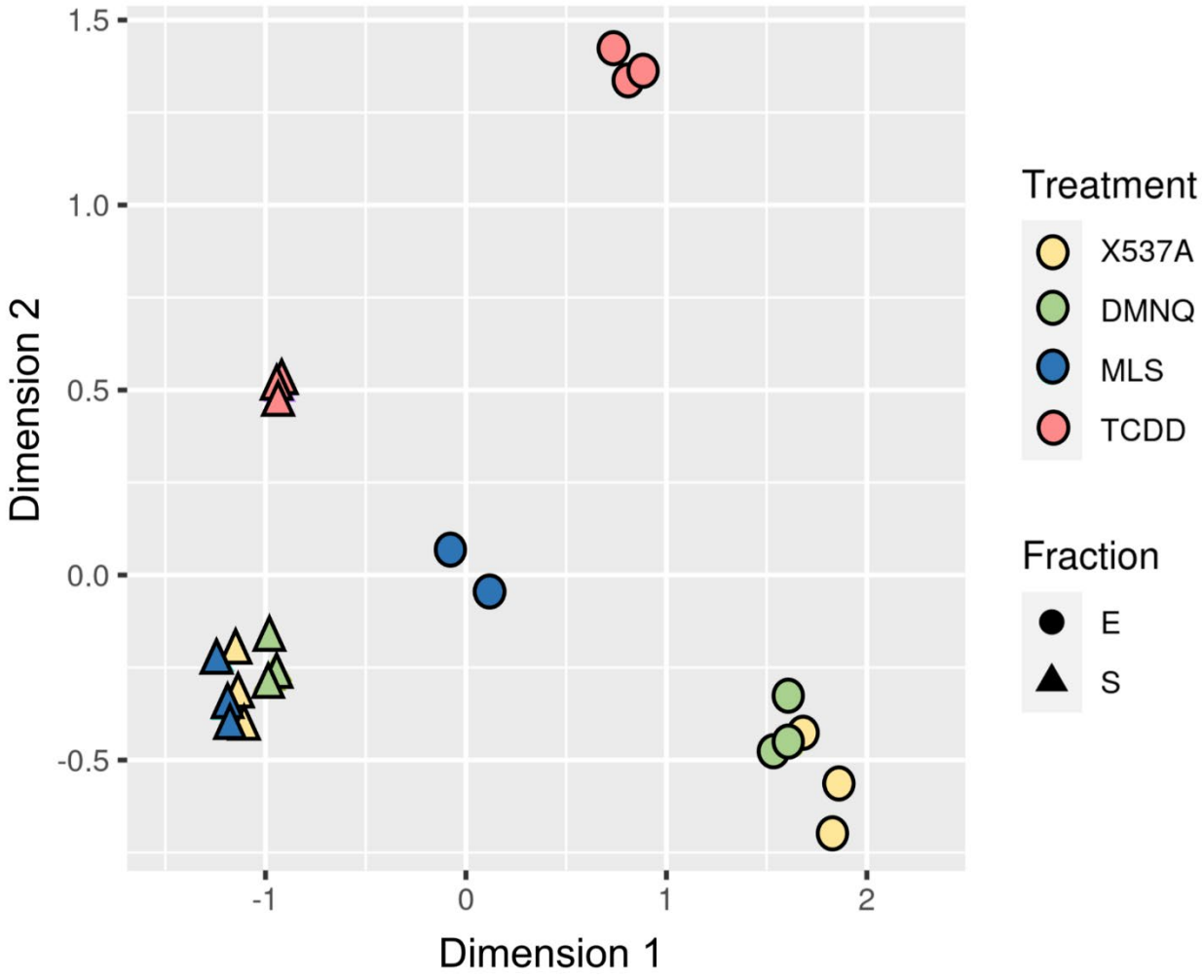

Figure 3. Multidimensional scaling (MDS) plot demonstrates the level of similarity of individual proteomic samples. The figure shows individual samples from three independent repeats except MLS-E. Due to errors in sample preparation, very few peptides were detected by the instrument and, therefore, one of the three MLS-E samples was excluded from the analysis. MDS coordinates were calculated using the function plotMDS from the edgeR Bioconductor package. E, envelope fraction. S, soluble fraction.

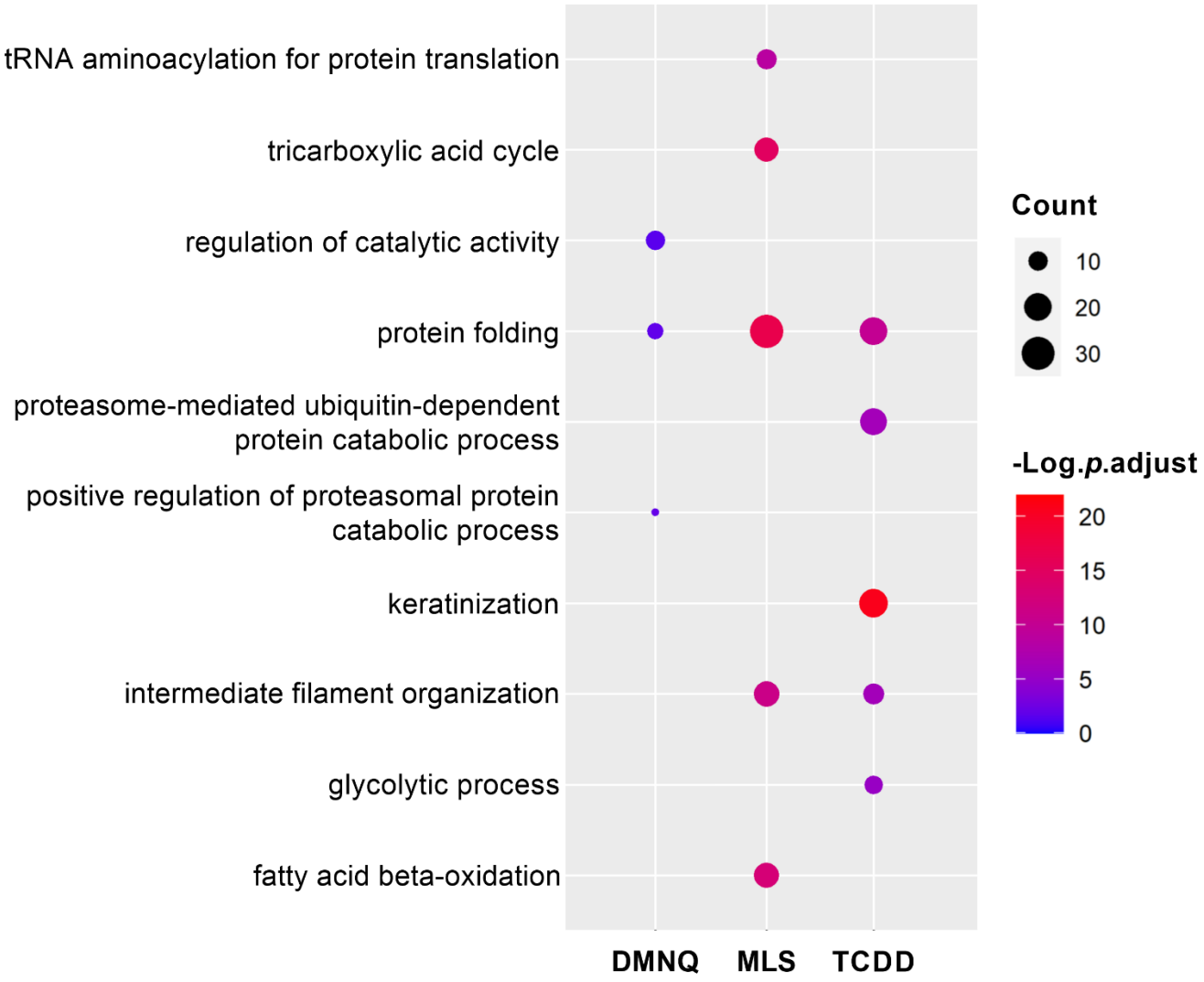

Figure 4. GO-BP enrichment analysis on proteins differentially enriched by DMNQ, MLS, and TCDD. Proteins with at least 2-fold increase ($p < 0.01$) compared to those in X537A-CEs were included for the analysis. Figure shows the top five significantly enriched GO-BP terms. Significance levels are presented as negative log10 *p*-value. Count, the number of proteins enriched in the corresponding term.

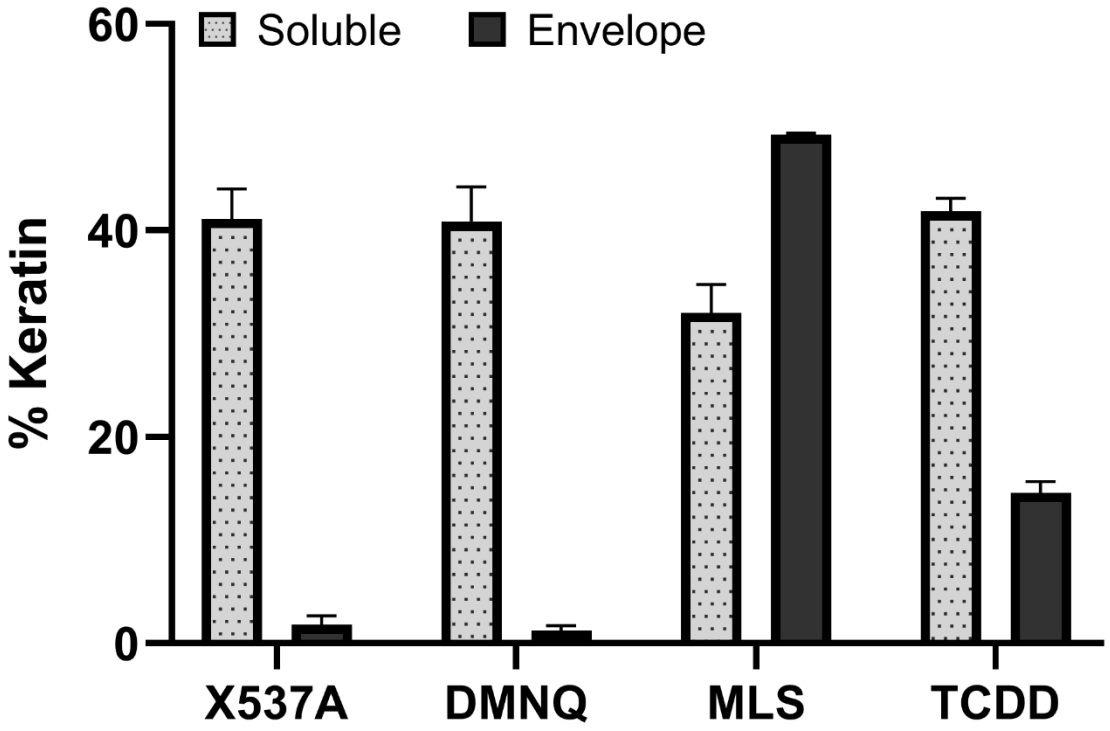

Figure 5. Keratin content in the cytosolic soluble and envelope fractions. The % of keratin in each group was calculated using estimates from emPAI abundance analysis.

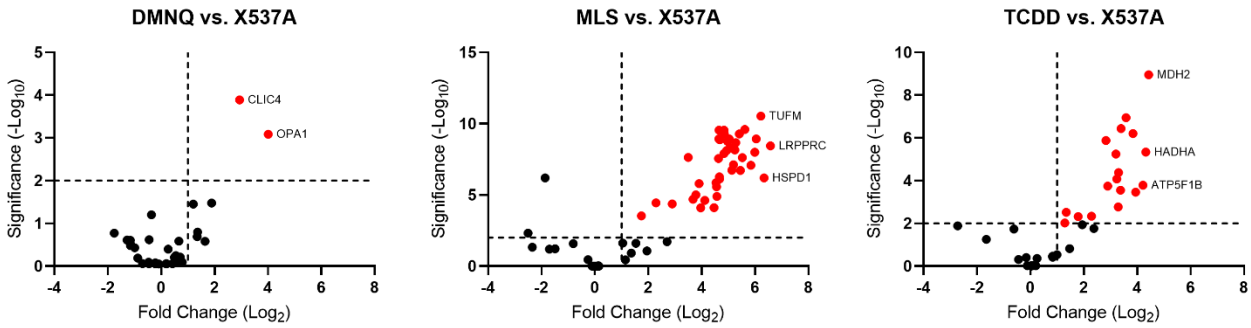

Figure 6. Altered Mt proteins in each comparison. Proteins labeled in red were ≥ 2-fold enriched by the ROS generators ($p < 0.01$). The vertical dashed line indicates 2-fold enrichment, and the horizontal dashed line indicates statistical significance with *p*-value of 0.01.

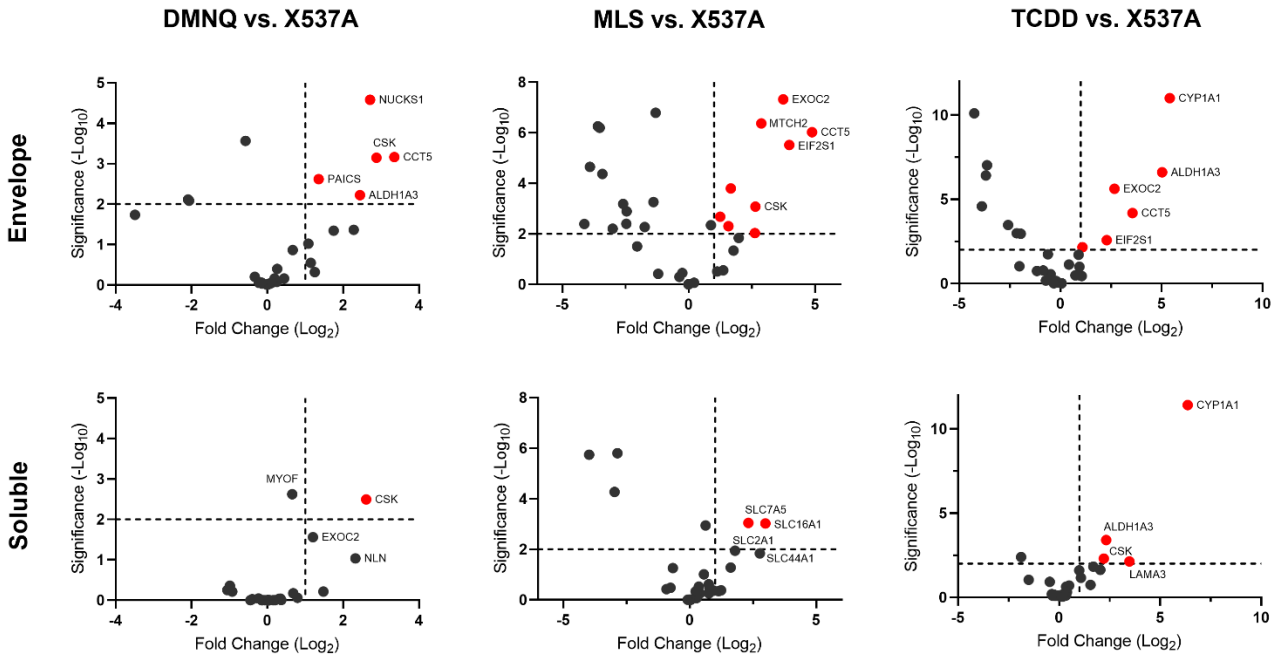

Figure 7. Altered proteins of AhR target genes in the cytosolic soluble and envelope fraction. Proteins labeled in red were ≥ 2-fold enriched by the ROS generators ($p < 0.01$). The vertical dashed line indicates 2-fold enrichment, and the horizontal dashed line indicates statistical significance with *p*-value of 0.01.